Nanoscale Res Lett (2010) 5:25–30
DOI 10.1007/s11671-009-9438-z

NANO EXPRESS

Magnetic Anisotropic Energy Gap and Strain Effect in Au Nanoparticles

Po-Hsun Shih · Sheng Yun Wu

Received: 1 April 2009 / Accepted: 9 September 2009 / Published online: 22 September 2009

Abstract We report on the observation of the size effect of thermal magnetization in Au nanoparticles. The thermal deviation of the saturation magnetization departs substantially from that predicted by the Bloch $T^{3/2}$-law, indicating the existence of magnetic anisotropic energy. The results may be understood using the uniaxial anisotropy Heisenberg model, in which the surface atoms give rise to polarized moments while the magnetic anisotropic energy decreases as the size of the Au nanoparticles is reduced. There is a significant maximum magnetic anisotropic energy found for the 6 nm Au nanoparticles, which is associated with the deviation of the lattice constant due to magnetocrystalline anisotropy.

Keywords Nanoparticles · Magnetic anisotropy · Magnetic properties · Spin waves

Introduction

Metal nanoparticles of Pd, Au, and Cu have been extensively studied, because, due to a reduction in dimensionality, their ferromagnetic polarizations are quite different from those observed in transition metals [1–6]. The most frequent effects of the small size are lattice rearrangement, crystalline imperfections, a higher degree of localization, and narrowed valence band width. It has been reported in previous studies [2, 4] that individual Pd and Au nanoparticles may reach their ferromagnetic moment at low temperatures, and that, theoretically, there may be a slight enhancement of the *4d* localization, although Pd and Au are both characterized by diamagnetism in the bulk state. Bulk Au metal also demonstrates a typical diamagnetic response of -1.42×10^{-6} emu/g [7], when the [Xe]$4f^{14}5d^{10}6\,s^{1}$ Au configuration has a closed *d* shell and a single *s* electron. Finite-size effects play a dominant role in determining the magnetic properties. A decrease in size can lead to unusual ferromagnetic and diamagnetic properties. The origin of the ferromagnetism observed in filled 4*d* or 5*d* electron nanoparticle systems can be explained as due to giant magnetic anisotropy [8] and Fermi-hole effects [9] that influence the evolution from the surface polarization spins to the diamagnetic bulk state. In this letter, we discuss the effects of surface polarization and weak magnetic anisotropy in Au nanoparticles, which indicate the appearance of ferromagnetic spin polarization and magnetic anisotropic energy at low temperatures. Moreover, the strain induced by the lattice can be used to tune the magnetic anisotropic energy, which is obtained from the quantum spin wave theory and the anisotropic Heisenberg ferromagnetic model.

Experimental Details

The Au nanoparticles used in the present study were fabricated by the thermal evaporation method. High-purity gold ingots (99.999%) were evaporated in the range of 0.1–2 T. The Ar gas was fed at a rate of $\sim$0.1 Å/s. To avoid contamination by magnetic impurities originating from the stainless steel plate the samples were collected by a rotating silicon substrate maintained at the temperature of liquid nitrogen. The resultant samples consisted of collections of individual Au nanoparticles in the form of dried powder. The morphology and structures of the prepared

P.-H. Shih · S. Y. Wu (✉)
Department of Physics, National Dong Hwa University, Hualien 97401, Taiwan
e-mail: sywu@mail.ndhu.edu.tw

nanoparticles were then characterized using transmission electron microscopy (TEM, JEM-1400 JEOL).

Results and Discussion

Structural Analysis

It is clearly evident in the portion of the TEM images shown in Fig. 1a that the nanoparticles are spherical and well separated. The interconnecting nanoparticles are stuck together in clusters due to electrostatic effects as well as an artifact of the drying of aqueous suspensions. The size and distribution of the nanoparticles can be calculated. An examination of the portion of the TEM image shown in the Fig. 1b clearly shows that size and distribution are quite asymmetric and can be described using a log-normal distribution function. The log-normal distribution is defined as follows: $f(d) = \frac{1}{\sqrt{2\pi}d\sigma}\exp\left(-\frac{(\ln d - \ln <d>)^2}{2\sigma^2}\right)$, where $<d>$ is the mean value and σ is the standard deviation of the function. The mean diameter and standard deviation obtained from the fits are $<d> = 3.7(9)$ nm and $\sigma = 0.251$, respectively. The small standard deviation ($\sigma < 0.5$) of the function indicates that the distribution is confined to a limited range. The broadening of the width of the distribution profile is due to crystalline and nanoparticle aggregation effects. The electron diffraction pattern corresponding to a selected area in the 3.7(9) nm Au nanoparticles is shown in Fig. 1c and clearly reveals the crystalline nature of the sample. The pattern of the main spots can easily be indexed as basically cubic in structure with a space group of $Fm-3m$ and a lattice parameter of $a = 4.07(4)$ Å. This is consistent with earlier data for bulk Au [7]. The diameters of the nanocrystals as determined from TEM images of the samples used in this study were approximately 3.7(9), 4.3(6), 5.6(4), 6.0(3), and 7.9(1) nm.

Magnetization

Magnetization measurements were performed using the conventional superconducting quantum interference device (Quantum Design, MPMS5) set up with magnetic fields from −5 to 5 T, covering a temperature range from 5 to 300 K. The Au nanoparticle sample was mounted in a sample holder capsule. Figure 2a shows the applied fields and the resultant magnetization of Au nanoparticles (with a mean diameter of 3.7(9) nm) obtained at the eight temperatures. When a lower field is applied the magnetization increases rapidly with the field; the increase follows a curved path, revealing that the magnetization follows a Langevin profile. At high temperatures, magnetization saturation is reached at around $H_a = 0.4$ T which is followed by a high-field linear decrease when the applied field H_a reaches 1.2 T. There are no significant differences in the magnetization measurements between the field-increasing and the field-decreasing loops found above 25 K, which are consistent with the superparamagnetic behaviors. Figure 2b shows the representative M(T) curves taken for the 3.7(9) nm Au nanoparticle assemblies at the selected applied magnetic field $H_a = 0.5$ T, revealing a superparamagnetic behavior that can be described by temperature dependence Langevin function. The resultant

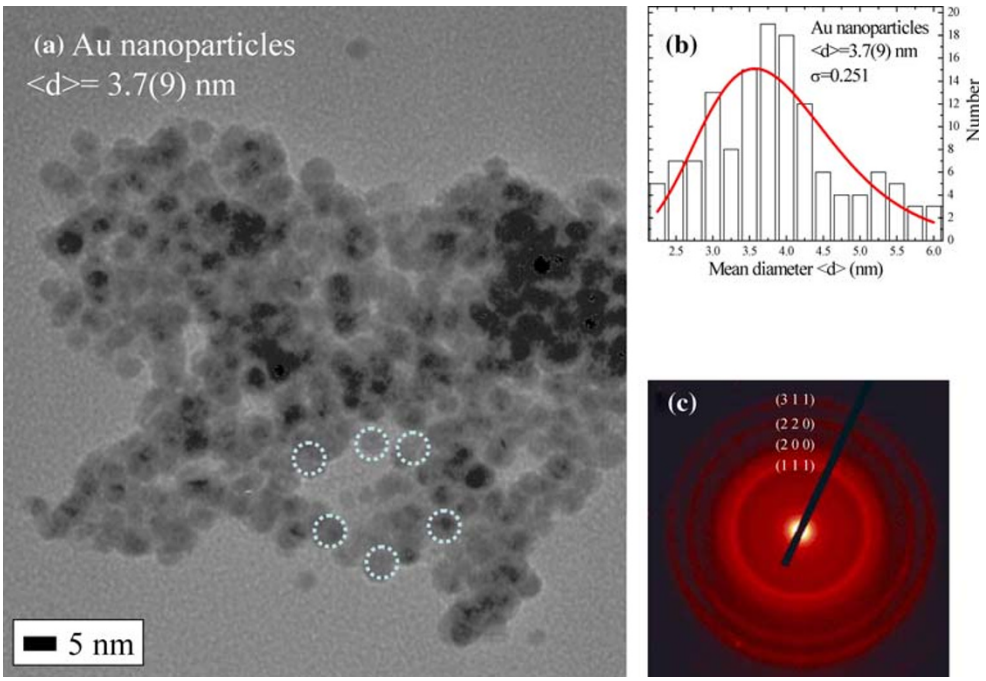

Fig. 1 **a** TEM images of Au nanoparticles; **b** size distribution obtained from a portion of a TEM image of Au nanoparticles, which can be described using a log-normal distribution function, as indicated by the *solid curve*; **c** electron diffraction patterns of a selected area 3.7(9) nm Au nanoparticles, revealing the cubic structure of the Au nanoparticles

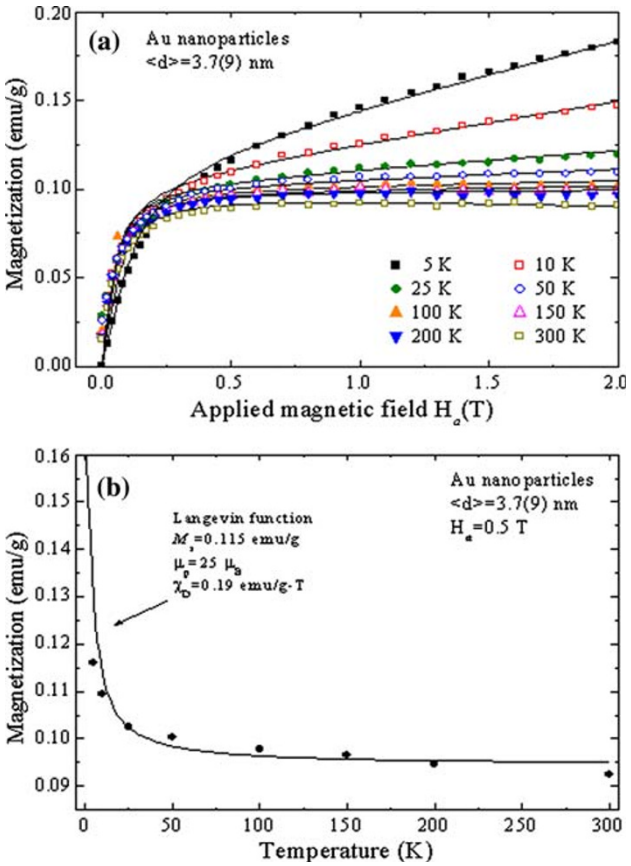

Fig. 2 **a** Effects of the various temperatures plotted in relation to the magnetization. The *solid lines* represent the fitted results. **b** Temperature dependence of the $M(T)$ curve taken for the 3.7(9) nm Au nanoparticle assemblies at the selected applied magnetic field $H_a = 0.5$ T

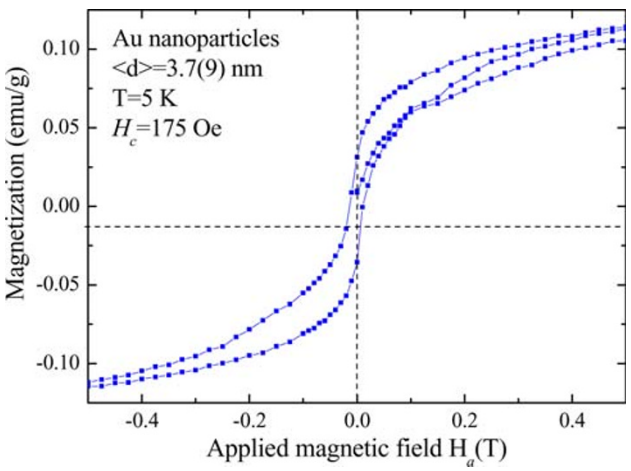

Fig. 3 Magnetization loops at 5 K for the 3.7(9) nm Au nanoparticles revealing the appearance of magnetic hysteresis in the low field regime

fitting parameters are shown in Fig. 2b. This suggests the existence of two different magnetic components in the sample—a superparamagnetic and a diamagnetic component. A representative hysteresis loop taken at 5 K is shown in Fig. 3. A distinguishable asymmetric coercivity $H_c = 175$ Oe can be observed in the low H_a regime, which signals the existence of ferromagnetic spin in the 3.7(9) nm Au nanoparticles. The value obtained for coercivity is close to other previously published values for similar Au nanoparticles [10]. The asymmetric characteristics are assumed to originate from competition between the unidirectional and uniaxial anisotropy [11, 12].

Consequently, we can describe the superparamagnetic system using a Langevin function in combination with a linear component associated with diamagnetism [13, 14]. The resultant total magnetization can be expressed as

$$M(H,T) = M_s L(x) + \chi_D H, x = \frac{\mu_p H}{k_B T}. \quad (1)$$

Here $L(x) = \coth(x) - 1/x$ is the Langevin function, M_s is the saturation magnetization, k_B is the Boltzmann's constant, and χ_D is the diamagnetic susceptibility term. The analysis relevant to Eq. 1 is based on a model which ignores the inter-particle interactions and the contributions of the distributions of the magnetic moment due to the log-normal size distribution of the nanoparticle system [15]. It can be seen that the fitted curves (solid line in Fig. 2a) are quite consistent with the experimental data. The mechanism often invoked to explain the occurrence of surface-spin polarization effects in nonmagnetic particles [4] is that the shell of the particle is ordered as a ferromagnetic shell, while the core of each Au nanoparticle still behaves as a diamagnetic single domain. Indeed, there is a discrepancy between the data and the Langevin profile shown in the *M(H)* curves taken at the low field regime. One possible cause of this difference in the fit is the production of a nonmagnetic surface layer by the chemical interaction between the particle and the oxidation. In light of the results obtained in various studies [16], we believe that this difference has a different origin. An alternate explanation has been made by Berkowitz [17, 18], who attributed the reduction in the expected magnetization at low temperature to difficulty in reaching saturation, because of a large surface anisotropy.

Magnetic Anisotropic Energy Gap

The thermal deviation of the saturation magnetization can be used to identify the anisotropic energy gap. Figure 4 shows the dependency of the thermal energy of the thermal deviation $\Delta M_s(T) = [M_s(5K) - M_s(T)]/M_{th}$ on the saturation magnetization, as obtained from the fitting of Eq. 1, where M_{th} is the saturated magnetization taken at room temperature. The $\Delta M_S(T)$ curve follows the Bloch $T^{3/2}$-law (dashed line) expected for ferromagnetic isotropic systems below 10 K [14, 19] but departs from the curve in the high

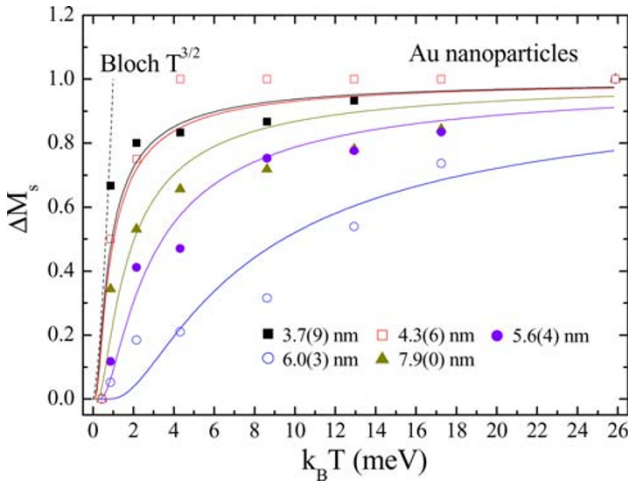

Fig. 4 Plot of the dependency of the thermal energy on the saturation magnetization $M_s(T)$ together with the thermal deviation $\Delta M_s(T)$ due to the saturation magnetization. The *solid lines* represent the fitted results

thermal energy regime, signaling the onset of magnetic anisotropy [15, 20–23], presumably due to the high surface-to-volume ratio of the nanoparticles. The discrepancy of fit above 10 K (for low applied fields) may be associated with the effects of uniaxial anisotropy [20–22] and with inhomogeneities in the magnetic moments [23], which have been ignored in the above analysis.

Here, we consider the surface and anisotropic effects in a quantum spin wave model for the Heisenberg ferromagnetic model [24, 25]. We can incorporate the spin–spin effects and anisotropy between coupling constants, that are known to be important in a nano-size system, into the anisotropic Hamiltonian, but do not include diamagnetic effects [26–28]

$$H = -\sum_{i,j}\left[J_z S_{iz}S_{jz} + J_{xy}(S_{ix}S_{jx} + S_{iy}S_{jy})\right] - mB\sum_i S_{iz}, \tag{2}$$

where the sum in the first term is the anisotropic ferromagnetic Heisenberg exchange interaction (J_z and J_{xy}) between nearest-neighbor spins on a nanoparticle; S denotes the spin component of the electrons; and the last part corresponds to the Zeeman energy (mS is the magnetic moment per atom). The theory and the method of calculation have already been described in detail elsewhere [26–28], therefore only a few basic steps will be given here. We utilize an external perturbation method and calculate the energy in the ground state of the spin wave with wave vector q and dispersion relation $\varepsilon_0(q)$. We can now rewrite the equation as

$$\varepsilon_0(q) = S\sum_{\delta}(J_z - J_{xy}e^{iq\cdot\delta}), \tag{3}$$

where δ is the nearest-neighbor vector. The lattice constants for Au face-centered cubic nanoparticles with $Fm-3m$ symmetry are $a = 4.07(4)$ Å, with a nearest-neighbor spacing of $\bar{a} = a/\sqrt{2}$. The dispersion relation can be rewritten as

$$\varepsilon_0(q) = 12S(J_z - J_{xy}) + 12SJ_{xy}\left[1 - \frac{1}{6}\left(\cos q_x\bar{a}\cos q_y\bar{a} + \cos q_x\bar{a}\cos q_z\bar{a} + \cos q_y\bar{a}\cos q_z\bar{a}\right)\right]. \tag{4}$$

This anisotropy in the coupling constants produces an energy gap in the spin wave spectrum of $\Delta = 12S(J_z - J_{xy})$. The gap leads to an exponential dependence of the order parameter on the thermal energy k_BT:

$$\Delta M_S(T) = [M_S(5K) - M_S(T)]/M_{th} \approx e^{-\frac{\Delta}{k_BT}}. \tag{5}$$

The solid lines indicate the results from the fit of Eq. 5; the fitting parameters are listed in Table 1; the energy gap obtained from the fit is plotted with the diameter in the Fig. 5a (right panel). In the case of 3.7(9) nm, at higher thermal energy $k_BT \sim 8$ meV, the monotonic change of ΔM_s is closed to one and will be overcame by the thermal energy. The direction of the magnetization of each Au nanoparticle simply follows the direction of the applied magnetic field. Consequently, the magnetization becomes superparamagnetic and shows paramagnetic properties.

Table 1 Summary of the size and fitting results for Au nanoparticles

<d> (nm)	M_s(5 K, emu/g)	M_{th}(emu/g)	Δ(meV)
3.7(9)	0.115	0.015	0.646
4.3(6)	0.058	0.004	0.709
5.6(4)	0.031	0.0085	2.391
6.0(3)	0.065	0.0076	6.527
7.9(1)	0.014	0.0032	1.412

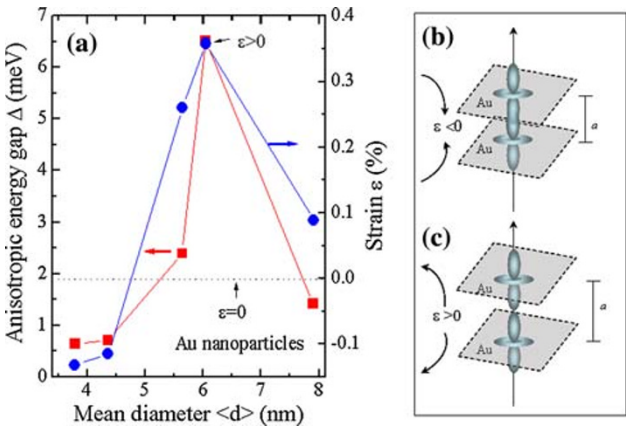

Fig. 5 **a** Plots of the variation in Δ and strain ε with mean diameter, revealing the increase in magnetic anisotropic energy with increasing particle size. **b** Schematic plots for negative strain ($\varepsilon < 0$), and **c** positive strain ($\varepsilon > 0$)

The larger the size of the nanoparticle, the higher the magnetic anisotropic energy, which therefore increases with increasing particle size, until reaching the maximum magnetic anisotropic energy: $\Delta = 6.527$ meV in the 6.0(3) nm Au nanoparticles. The results are in good agreement with the molecular field theories, which predict linear or exponential variations for large and small anisotropic energies, depending on whether a classical or quantized system is used for the magnetic moment [29]. In general, magnetic anisotropy means the dependence of the internal energy of a system on the direction of the spontaneous magnetization. Most kinds of magnetic anisotropy are related to the deviations in the lattice constant of the strain, known as magnetocrystalline anisotropy [30]. Figure 5 shows the strain as a function of mean diameter <d>. Shown in Fig. 5b (left panel), the relative strain can be estimated from the change in the *a*-axis lattice constant of Au nanoparticles

$$\varepsilon(\%) = \frac{a - a_0}{a_0}(\times 100\%), \tag{6}$$

where a and a_0 (4.076 Å for bulk Au) indicate the lattice constants of the strained and unstrained crystal, respectively. In general, the spin–orbit interaction will induce a small orbital momentum, which couples the magnetic moment to the crystal axes. In a negative strained nanocrystalline system, the wavefunctions between neighboring atoms will overlap and reduce the magnetic anisotropy. A reduction in the size of the nanoparticles ($\varepsilon < 0$) results in unit cell contraction, which increases the stability of the higher symmetry lattice and the coupling strength of wavefunctions, shown in Fig. 5b. In a positive strained $\varepsilon > 0$ nanocrystalline system, shown in Fig. 5c, the lattice expands and decreases the coupling of wavefunctions. In the case of our Au nanoparticles, the maximum positive deviation in strain was observed when the mean size was 6.0(3) nm. The tendency of strain of size effects was similar with the results of anisotropic energy. However, one possible explanation for the higher strain state accompany with higher magnetic anisotropy energy is an indicative of lattice- and magnetic-anisotropy for Au nanoparticles.

Conclusions

An analysis of the results leads to an interesting conclusion: that nanosized transition metal Au particles exhibit both ferromagnetism and superparamagnetism, which are in contrast to the metallic diamagnetism characteristic of bulk Au. The superparamagnetic component of Au nanoparticles shows an anomalous temperature dependence that can be well explained by the modified Langevin function theory. Weak magnetic anisotropy was observed in the mean deviation magnetization. The energy of the magnetic anisotropic can be determined from the fitting of the anisotropic Heisenberg model and related with the change of strain. One possible explanation for the origin of the observed superparamagnetic component of the magnetization would be the existences of non-localized holes and charge transfer which would signify that deviation from stoichiometry would make only a small paramagnetic contribution to the magnetization [31].

Acknowledgments We appreciate the financial support of this research from the National Science Council of the Republic of China under grant No. NSC-97-2112-M-259-004-MY3.

References

1. T. Teranishi, I. Kiyokawa, M. Miyake, Adv. Mater. **10**, 596 (1998)
2. H. Hori, T. Teranishi, Y. Nakae, Y. Seino, M. Miyake, S. Yamada, Phys. Lett. A **263**, 406 (1999)
3. W.-H. Li, S.Y. Wu, C.C. Yang, S.K. Lai, K.C. Lee, H.L. Huang, H.D. Yang, Phys. Rev. Lett. **89**, 135504 (2002)
4. Y. Yamamoto, T. Miura, M. Suzuki, N. Kawamura, H. Miyagawa, T. Nakamura, K. Kobayashi, T. Teranishi, H. Hori, Phys. Rev. Lett. **93**, 116801 (2004)
5. H. Hori, Y. Yamamoto, T. Iwamoto, T. Miura, T. Teranishi, M. Miyake, Phys. Rev. B **69**, 174411 (2004)
6. P. Crespo, R. Litrán, T.C. Rojas, M. Multigner, J.M. de la Fuente, J.C. Sánchez-López, M.A. García, A. Hernando, S. Penadés, A. Fernández, Phys. Rev. Lett. **93**, 087204 (2004)
7. J.W. Shih, Phys. Rev. **38**, 2051 (1931)
8. A. Hernando, P. Crespo, M.A. García, Phys. Rev. Lett. **96**, 057206 (2006)
9. M.K. Harbola, V. Sahni, Phys. Rev. B **37**, 745 (1988)
10. J.S. Garitaonandia, M. Insausti, E. Goikolea, M. Suzuki, J.D. Cashino, N. Kawamura, H. Ohsawa, I.G. de Muro, K. Suzuki, F. Plazaola, T. Rojo, Nano Lett. **8**, 661 (2008)
11. J. Chen, G. Jin, Y.-Q. Ma, J. Phys. Condens. Matter **19**, 236225 (2007)
12. C. Xu, Z.Y. Li, P.M. Hui, J. Appl. Phys. **89**, 3403 (2001)
13. C.P. Bean, J.D. Livingston, J. Appl. Phys. **30**, S120 (1959)
14. C. Kittel, *Introduction to solid state physics* (Wiley, New York, 1996)
15. R.W. Chantrell, J. Popplewell, S.W. Charles, IEEE Trans. Magn. **MAG-14**, 975 (1978)
16. J. Popplewell, S.W. Charles, IEEE Trans. Magn. **MAG-17**, 2923 (1981)
17. Y.W. Du, H.X. Lu, Y.Q. Wang, T.X. Wang, J. Magn. Magn. Mater. **31**, 896 (1983)
18. A.E. Berkowitz, J.A. Lahut, I.S. Jacobs, L.M. Levinson, D.W. Forester, Phys. Rev. Lett. **34**, 594 (1975)
19. K. Mandal, S. Mitra, P.A. Kumar, Europhys. Lett. **75**, 618 (2006)
20. M. El-Hilo, R.W. Chantrell, K. O'Grady, J. Appl. Phys. **84**, 5114 (1998)
21. F. Wiekhorst, E. Shevchenko, H. Weller, J. Kötzler, Phys. Rev. B **67**, 224416 (2003)
22. S.R. Hoon, D.B. Lambrick, J. Phys. Confer. Ser. **17**, 1 (2005)
23. N.J.O. Silva, V.S. Amaral, L.D. Carlos, Phys. Rev. B **71**, 184408 (2005)
24. F.J. Dyson, Phys. Rev. **102**, 1217 (1956)
25. S. Katsura, Phys. Rev. **127**, 1508 (1962)

26. P.V. Hendriksen, S. Linderoth, P.-A. Lindgård, Phys. Rev. B **48**, 7259 (1993)
27. P.V. Hendriksen, S. Linderoth, P.-A. Lindgård, J. Phys. Condens. Matter **5**, 5675 (1993)
28. M. Plischke, B. Bergersen, *Equilibrium statistical physics* (World Scientific, Singapore, 1994), p. 393
29. P.L. Taylor, *A Quantum approach to the solid state* (Prentice Hall, New Jersey, 1970)
30. L.F. Yin, D.H. Wei, N. Lei, L.H. Zhou, C.S. Tian, G.S. Dong, X.F. Jin, L.P. Guo, Q.J. Jia, R.Q. Wu, Phys. Rev. Lett. **97**, 067203 (2006)
31. D.K. Stevens, J.W. Cleland, J.H. Crawford, H.C. Schweinler, Phys. Rev. **100**, 1084 (1955)